IJC
International Journal of Cancer

ONECUT2 upregulation is associated with CpG hypomethylation at promoter-proximal DNA in gastric cancer and triggers *ACSL5*

Eun-Hye Seo[1,2], Hee-Jin Kim[1], Jong-Hwan Kim[3], Byungho Lim[4], Jong-Lyul Park[1], Seon-Young Kim[2,3], Sang-Il Lee[5], Hyun-Yong Jeong[6], Kyu-Sang Song[7] and Yong-Sung Kim[1,2]

[1]Genome Editing Research Center, Korea Research Institute of Bioscience and Biotechnology, Daejeon, Republic of Korea
[2]Department of Functional Genomics, Korea University of Science and Technology, Daejeon, Republic of Korea
[3]Personalized Genomic Medicine Research Center, Korea Research Institute of Bioscience and Biotechnology, Daejeon, Republic of Korea
[4]Division of Drug Discovery Research, Research Center for Drug Discovery Technology, Korea Research Institute of Chemical Technology, Daejeon, Republic of Korea
[5]Department of Surgery, College of Medicine, Chungnam National University, Daejeon, Republic of Korea
[6]Department of Internal Medicine, College of Medicine, Chungnam National University, Daejeon, Republic of Korea
[7]Department of Pathology, College of Medicine, Chungnam National University, Daejeon, Republic of Korea

Many studies have focused on global hypomethylation or hypermethylation of tumor suppressor genes, but less is known about the impact of promoter hypomethylation of oncogenes. We previously showed that promoter methylation may gradually increase or decrease during the transition from gastric mucosa (GM) to intestinal metaplasia (IM) to gastric cancer (GC). In our study, we focused on regional CpG hypomethylation of the promoter-proximal DNA of the transcription factor *ONECUT2* (*OC2*) in IM and GC cells. We validated the hypomethylation of promoter-proximal DNA of *OC2* in 160 primary GCs, in which methylation level correlated negatively with *OC2* mRNA level. IM and GC cells stained positively for OC2, whereas GM cells did not. Stable transfection of *OC2* in GC cells promoted colony formation, cell migration, invasion and proliferation. Moreover, *OC2* knockdown with a short hairpin RNA suppressed tumorigenesis in nude mice. In addition, chromatin immunoprecipitation coupled with DNA sequencing and RNA-seq analyses revealed that *OC2* triggered *ACSL5*, which is strongly expressed in IM of the stomach but not in GM, indicating that *OC2* and *ACSL5* are early-stage biomarkers for GC. We also observed a high correlation between the levels of *OC2* and *ACSL5* mRNAs in the GENT database These results suggest that epigenetic alteration of *OC2* upregulates its expression, which then activates *ACSL5*; thus, *OC2* is induced in IM by epigenetic alteration and triggers *ACSL5* expression, and thus *OC2* and *ACSL5* may cooperatively promote intestinal differentiation and GC progression.

Introduction

Gastric cancer (GC) is currently the fourth most common cancer worldwide and is the second leading cause of cancer mortality globally, with over 700,000 deaths each year.[1] Thus, a pressing need exists for useful biomarkers that define the malignancy potential of primary gastric tumors, inform prognosis, and could

Additional Supporting Information may be found in the online version of this article.

Key words: gastric cancer, intestinal metaplasia, DNA hypomethylation, *ONECUT2*, *ACSL5*

Abbreviations: 5-aza-dC: 5-aza-2-deoxycytidine; ACSL5: acyl-CoA synthetase long-chain family member 5; CDX2: caudal type homeobox 2; CFB: complement factor B; ChIP: chromatin immunoprecipitation; CNUH: Chungnam National University Hospital; DGC: diffuse-type GC; DMP: differentially methylated promoter; GC: gastric cancer; GENT: Gene Expression across Normal and Tumor tissue; GEO: Gene Expression Omnibus; GM: gastric mucosa; *H. pylori*: *Helicobacter pylori*; *HNF6*: *hepatocyte nuclear factor 6*; IGC: intestinal-type GC; IM: intestinal metaplasia; KD: knockdown; NCBI: National Center for Biotechnology Information; *OC1–OC3*: *ONECUT1* through *ONECUT3*; PCR: polymerase chain reaction; qRT-PCR: quantitative reverse transcription PCR; RRBS: reduced representation bisulfite sequencing; SD: standard deviation; shRNA: short hairpin RNA; siRNA: small interfering RNA; TCGA: The Cancer Genome Atlas; TSS: transcription start site; UCSC: University of California, Santa Cruz

DOI: 10.1002/ijc.32946
History: Received 7 Jun 2019; Accepted 19 Feb 2020; Online 4 Mar 2020

Correspondence to: Yong-Sung Kim, E-mail: yongsung@kribb.re.kr

What's new?

DNA hypomethylation can promote cancer development through activation of genes with oncogenic potential. Here, the authors found that CpGs in the promoter-proximal DNA of *ONECUT2* were hypomethylated in intestinal metaplasia and gastric cancers, and that hypomethylation was associated with *ONECUT2* upregulation. Functional analysis demonstrated that *ONECUT2* has oncogenic potential and could activate *ACSL5*, which is also expressed in intestinal metaplasia, suggesting that *ONECUT2* and *ACSL5* may cooperate to promote intestinal differentiation or development of gastric cancer. Taken together, the findings suggest that *ONECUT2* and its downstream target *ACSL5* could be used to develop early detection biomarkers and prevent gastric carcinogenesis.

assist in establishing new therapeutic and preventive strategies for this disease. Gastric carcinogenesis can manifest only after a gradual accumulation of various genetic and epigenetic alterations. Among epigenetic alterations, there has been great interest in the direct hypermethylation of tumor suppressor genes.[2] It has been commonly asserted that DNA hypomethylation can also promote cancer development through activation of genes with oncogenic potential,[3] although examples of oncogenes that truly rely on DNA hypomethylation for activation in tumors have not been published. However, recent advances in global methylation profiling suggest that aberrant promoter hypomethylation is a frequent event in hematologic malignancies, such as a chronic lymphocytic leukemia.[4]

To pursue hypomethylation targets associated with gastric carcinogenesis, we previously performed a reduced representation bisulfite sequencing (RRBS) analysis using DNA samples from gastric mucosa (GM), intestinal metaplasia (IM) and GC cells from one patient with intestinal-type GC (IGC).[5] Regional hypomethylation was found in the promoter-proximal DNA of *ONECUT2* (*OC2*; also called hepatocyte nuclear factor 6B or *HNF6B*) in IM and GC cells. The *ONECUT* family in mammals comprises three members: *OC1* (also called *HNF6A*), *OC2* and *OC3*. The encoded proteins activate genes involved in controlling cell differentiation in liver and pancreas as well as patterning of trigeminal sensory neurons.[6] Although a role for *OC2* in cancer is not well defined, it was recently reported that *OC2* is associated with the development of colorectal cancers.[7] More recent work showed that *OC2* is hyperactivated in a substantial subset of human prostate cancers and therefore is a potential drug target for the metastatic phase of aggressive prostate cancers.[8] The biological role, if any, of *OC2* in GC has not yet been examined.

To address this shortcoming in knowledge, we investigated the molecular mechanism responsible for regulation of *OC2* expression in GCs and elucidated its role in gastric carcinogenesis. Our results reveal that regional CpGs in the promoter-proximal DNA of *OC2* are predominantly hypomethylated in primary GCs and that the extent of methylation correlates negatively with *OC2* expression. Functional analysis revealed that *OC2* has oncogenic potential in GC cells and activates expression of acyl-CoA synthetase long-chain family member 5 (*ACSL5*), which is strongly expressed in IM but not GM. Our results suggest that *OC2* and *ACSL5* are markers for IM in the stomach that may play important roles in intestinal differentiation or GC development and may be useful as targets for prevention of GC development or as therapeutics for GC.

Materials and Methods

Cell lines and tissue samples

Sixteen GC cell lines (Fig. 4*a*), including SNU001 (RRID: CVCL_0099), SNU005 (CVCL_0078), SNU016 (CVCL_0076), SNU216 (CVCL_3946), SNU484 (CVCL_0100), SNU520 (CVCL_5072), SNU601 (CVCL_0101), SNU620 (CVCL_5079), SNU638 (CVCL_0102), SNU668 (CVCL_5081), SNU719 (CVCL_5086), AGS (CVCL_0139), KATOIII (CVCL_0371), MKN01 (CVCL_1415), MKN45 (CVCL_0434), MKN74 (CVCL_2791), were obtained from the Korean Cell Line Bank (http://cellbank.snu.ac.kr/main/index.html) and cultured in RPMI 1640 medium supplemented with 10% fetal bovine serum and 1% antibiotic-antimycotic solution (Invitrogen, Carlsbad, CA). All experiments were performed with mycoplasma-free cells. And all GC cell lines have been authenticated using STR profiling within the last 3 years. The origin and characteristics of 16 gastric cancer cell lines were summarized in Supporting Information Table S1. One hundred sixty frozen tumors paired with adjacent nontumor tissues were provided by the Biobank of Chungnam National University Hospital (CNUH), a member of the Korea Biobank Network. All samples were obtained with informed consent, and their use was approved by the Internal Review Board at CNUH.

Bisulfite sequencing

Genomic DNA from GC cells or tissues was modified by sodium bisulfite using the EZ DNA Methylation kit (Zymo Research, Orange, CA). Bisulfite-modified DNA was amplified in a 20-μl reaction with primers (Supporting Information Table S2) for bisulfite sequencing region 1 (BS-R1) around the transcription start site (TSS) and BS-R2 in the promoter-proximal DNA or exon 1 of *OC2* (Fig. 1*d*). PCR products were cloned using the pGEM-T Easy vector (Promega, Madison, WI), and 10 clones were randomly chosen for sequencing. The methylation percentage for each sample was calculated as the number of methylated CpG dinucleotides among the total number of CpGs.

Reverse transcription-PCR and real-time quantitative RT-PCR

Total RNA was isolated from GC cells or tissues using the RNeasy kit (Qiagen, Valencia, CA), treated with DNase I (Promega), and

reverse-transcribed with Superscript II reverse transcriptase (Invitrogen) as previously described.[5] RT-PCR for *OC2* was performed as follows: 94°C for 5 min, followed by 35 cycles of 94°C for 30 sec, 64°C for 30 sec and 72°C for 30 sec, with a final cycle of 72°C for 7 min. *β-Actin* served as the PCR control. The PCR products were analyzed on 1.5% agarose gels stained with ethidium bromide. The primer sequences for RT-PCR are listed in Supporting Information Table S2. Real-time qRT-PCR for *OC2* was performed using a C1000 Thermal Cycler (Bio-Rad, Hercules, CA). cDNA (100 ng) was amplified as noted above by 45 cycles with 2× SYBR Green Supermix (Bio-Rad). *β-Actin* was amplified as a control. The relative amount of target mRNA was quantified using comparative threshold cycle (Ct) methods.

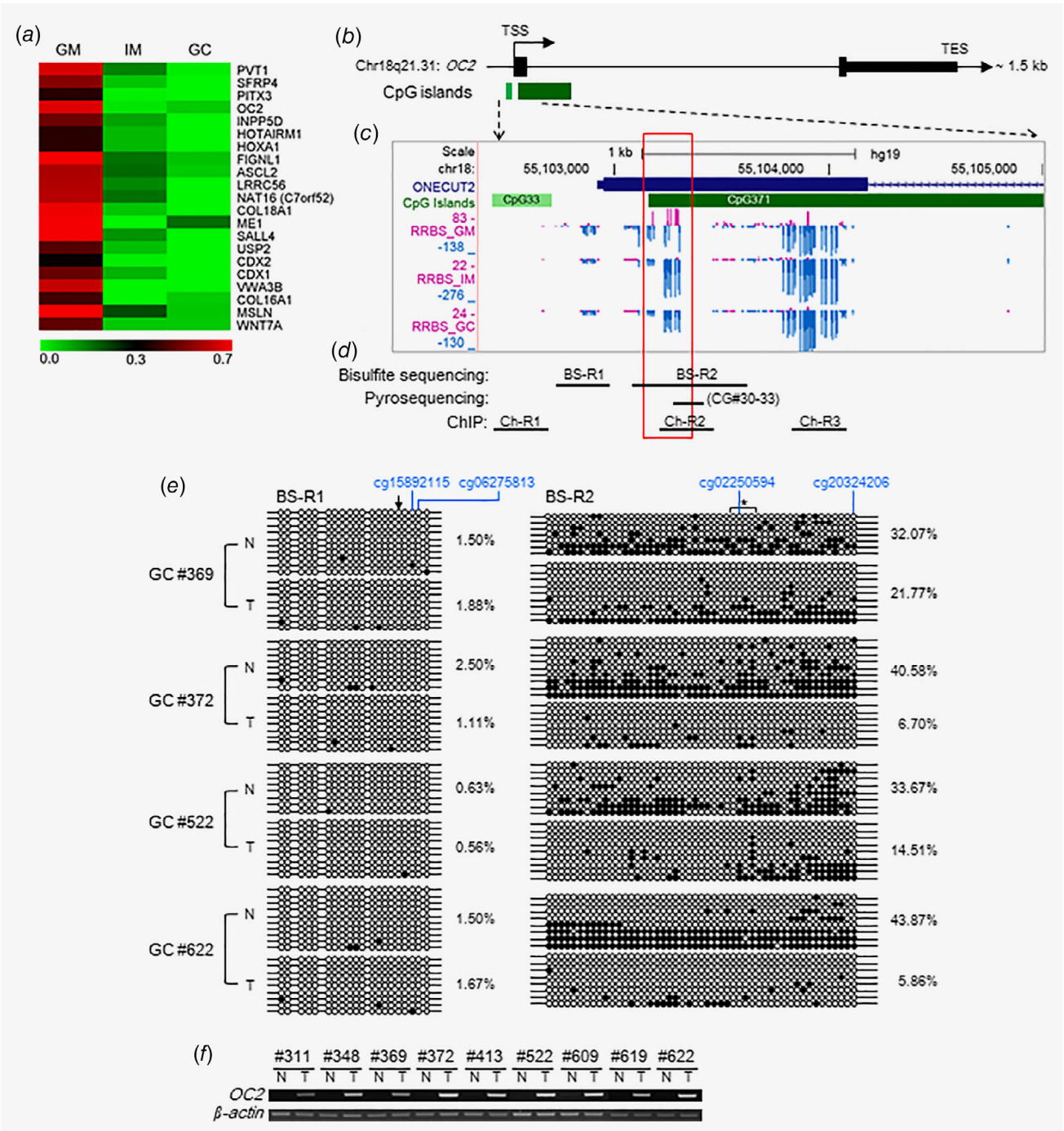

Figure 1. Legend on next page.

Pyrosequencing

Four CpG sites in BS-R2 (Fig. 1*d*) were selected for the quantification of the extent of methylation. Bisulfite-modified DNA (100 ng) was amplified by PCR in a 20-μl reaction using 2× Dye Mix polymerase (Enzynomics, Daejeon, Korea) to yield a 199-bp product using the primer set shown in Supporting Information Table S2. PCR was performed using an initial melting step of 94°C for 5 min, followed by 40 cycles of 94°C for 30 sec, 59°C for 30 sec and 72°C for 30 sec, with a final incubation at 72°C for 7 min. Pyrosequencing was performed as described[9] using the sequencing primer in Supporting Information Table S2 and the PSQ HS 96A System (Biotage AB, Kungsgatan, Sweden).

Immunohistochemistry

Immunohistochemical staining for *OC2* was performed with human gastric tissues containing GM, IM and GC regions using the streptavidin-biotin labeling method after microwave-assisted antigen retrieval. Briefly, formalin-fixed, paraffin-embedded 4-μm-thick sections were dewaxed in xylene, rehydrated through a graded series of alcohol, and placed in an endogenous peroxidase block for 15 min. Sections were then washed in water before antigen retrieval, placed in a citrate buffer and microwaved for 10 min. An *OC2*-specific monoclonal antibody (Thermo Fisher, Waltham, MA; diluted 1:300) was then applied, and antibody binding was detected using an avidin–biotin–peroxidase complex kit (Vector Laboratories, Burlingame, CA) using diaminobenzidine tetrahydrochloride solution (Biogenex, San Ramon, CA).

Chromatin immunoprecipitation assay

Chromatin immunoprecipitation (ChIP) assays were performed with GC cells for ChIP-PCR analysis or with *OC2*-expressing and control cells following a protocol from the Myers' laboratory (http://hudsonalpha.org/myers-lab/protocols) with modifications. Specifically, cells were fixed with 1% formaldehyde, lysed, and sonicated using a Covaris M220 (Covaris, Woburn, MA). For ChIP-PCR analysis, the sonicated lysates for GC cells were used by dividing the same amount into three tubes and 10% input. Normal Rabbit IgG (2 μg; Sigma-Aldrich), Anti-trimethyl-Histone H3 (Lys4) (2 μg; Sigma-Aldrich) and Anti-trimethyl-Histone H3 (Lys27) (2 μg; Sigma-Aldrich) was prebound to 20 μl Dynabeads coupled with protein A or protein G (Invitrogen). One microliter of each sample was used, and PCR was performed in three regions around the *OC2* TSS (Fig. 1*d*). The PCR products were analyzed on 1.5% agarose gels stained with ethidium bromide. The primer sequences for RT-PCR are listed in Supporting Information Table S2.

For ChIP-seq analysis, the sonicated lysate for *OC2*-expressing and control cells were used by dividing the same amount into two tubes and 10% input. Anti-*OC2* (10 μg; Proteintech, Rosemont, IL) was prebound to 50 μl Dynabeads coupled with protein A or protein G (Invitrogen). For *OC2*-expressing and control cells, genomic libraries with ~250- to 400-bp fragment sizes were generated with the input and *OC2*-immunoprecipitated fragments using the TruSeq ChIP Sample Prep kit (Illumina, San Diego, CA) and sequenced using the NextSeq_500 (Illumina), producing 76-bp single reads. Sequencing reads from ChIP-seq were aligned on human reference genome (hg19) using Bowtie2 software (version 2.2.2).[10] ChIP peak calling was performed using a Hypergeometric Optimization of Motif EnRichment (Homer, version 4.8.2),[11] and ChIP peak annotation was performed using the annotatePeaks module of Homer. ChIP peaks within the −1.0 to +1.0 kb region relative to TSSs were considered *OC2* binding sites in the promoters of corresponding genes. Consensus motifs were analyzed within a ±100 bp region on either side of the peaks.

Treatment of cells with 5-aza-dC and trichostatin A

Cells were seeded at a density of 1×10^6 per 100-mm dish, cultured for 24 or 72 hr, and treated with 1 μM 5-aza-2-deoxycytidine (5-aza-dC; Sigma-Aldrich, St. Louis, MO) to achieve demethylation and then 0.5 μM trichostatin A (Sigma-Aldrich) to inhibit histone deacetylase. After 2–5 days, cells were washed with PBS, and total RNA was extracted. Real-time qRT-PCR for *OC2* was performed as described above. Independent triplicate experiments were performed.

Figure 1. Methylation profile of early-onset hypomethylated DMPs and methylation signatures at promoter-proximal DNA of *OC2*. (*a*) Heat map of selected early-onset hypomethylated DMPs showing relative frequencies of methylated reads to total reads around gene promoters in GM, IM and GC cells from RRBS analysis. (*b*) Gene structure of *OC2* on human chromosome 18q21.31. Map was modified from the UCSC Genome Browser (http://genome.ucsc.edu). The distance from TSS to TES is ~1.5 kb. TSS, transcription start site; TES, transcription end site; thick black bars, exons; thin black bars, 5′- or 3′-untranslated regions; green bars, CpC islands containing 33 and 371 CpGs, respectively. (*c*) RRBS methylome profiles around the enlarged *OC2* exon1 DNA in paired GM, IM and GC cells from mirroring UCSC Genome Browser (hg19). Vertical lines indicate methylation scores of individual CpGs: Methylation and unmethylation scores are displayed as purple upward and blue downward bars. Red rectangle highlights differentially methylated region in GM compared to IM or GC. (*d*) Strategy for analysis in our study. Bisulfite sequencing was performed at promoter region BS-R1 (20 CpGs, −117–41 nt from TSS) and the promoter-proximal region BS-R2 (49 CpGs, 209–685 nt). Pyrosequencing was performed at four CpGs (#30–33) between 418 and 448. ChIP was performed at Ch-R1 (−451 to −270 nt), Ch-R2 (356–541 nt), and Ch-R3 (1,014–1,194 nt). (*e*) Bisulfite sequencing was performed with four paired GC tissues (#369, 372, 522 and 622; N, normal; T, tumor). Black and white circles indicate methylated and unmethylated CpG sites, respectively. Each row represents a single clone. Numbers on the right represent mean percentage of CpG sites that were methylated in each sample tissue. Four CpG sites (blue colored) in top indicate CpG positions examined in Figures 2*a* and 2*b*. Arrow in top left indicates TSS. Asterisk in top right indicates four CpG sites used for pyrosequencing. (*f*) RT-PCR in clinical tissues. *OC2* expression was examined in nine paired gastric tumor tissues, including the four paired tissues used for bisulfite sequencing. *β*-Actin was used as an internal control.

Establishment of stable cell lines

To establish *OC2*-expressing cell lines, the *OC2* coding sequence was amplified from cDNA prepared from SNU719 cells by PCR using the primers *Xba*I-*OC2*-F and *Not*I-*OC2*-R (Supporting Information Table S2) and then cloned into vector pCDH-CMV-MCS-EF1-Puro. For lentivirus construction, 293T cells were cotransfected with MISSION Lentiviral Packaging Mix plus empty vector or *OC2*-expressing vector. *OC2*-knockdown (*OC2*-KD) cells were established using TRCN0000013444 and TRCN0000013446 (*OC2*_sh#3 and *OC2*_sh#4, respectively; Sigma-Aldrich), targeting *OC2* mRNA. For lentivirus construction, 293T cells were cotransfected with MISSION Lentiviral Packaging Mix and control or *OC2* short hairpin RNA (shRNA) vectors. Cells for ectopic expression or KD experiments were seeded onto six-well culture plates. After 24 hr, supernatants containing the lentivirus were collected from the 293T cells, filtered, and applied to the target cells for lentiviral transduction. After 72 hr, the medium was changed to RPMI medium containing 1 μg/ml puromycin (Sigma-Aldrich). After 2 weeks of puromycin selection, the change in expression was confirmed by western blotting and qRT-PCR.

Western blotting

SDS-PAGE was conducted using a Bio-Rad western blotting system and a 10% acrylamide gel. Proteins were transferred to a polyvinylidene fluoride western blotting membrane (Sigma-Aldrich) and probed with anti-*OC2* (Abcam, Cambridge, UK) followed by mouse anti-rabbit IgG conjugated with horseradish peroxidase (Santa Cruz Biotechnology, Dallas, TX). Immunopositive bands were visualized using the enhanced luminescence image analyzer LAS-4000 (FUJI Film, Tokyo, Japan).

Cell proliferation and colony-forming assays

For cell proliferation assays, 2×10^3 cells were plated in a 96-well plate, and the proliferation over a given time course was measured with the EZ-Cytox Cell Viability Assay kit (ItsBio, Seoul, Korea) using a microplate reader (Molecular Devices, San Jose, CA) at 450 nm. For colony-forming assays, 5×10^2 cells were plated in a six-well plate. After 2 weeks, colonies were stained with crystal violet (0.5% crystal violet, 3.7% formaldehyde, 30% ethanol) and counted.

Cell migration and invasion assays

Cell migration and invasion were examined in transwell chambers (6.5-mm diameter, 8-μm pore size; Corning, Corning, NY). Cells (2×10^4) were added to the upper chamber, which contained 0.5 ml RPMI 1640 medium supplemented with 10–20% fetal bovine serum and 1% antibiotic–antimycotic solution (Invitrogen). For invasion assays, the transwell membrane was coated with 1 mg/ml Matrigel. Cells were incubated for 24 hr at 37°C, and nonmigrating or noninvading cells were removed with cotton swabs. Cells migrating to or invading the bottom of the membrane were stained with crystal violet and counted. For each well, three microscopic fields were chosen randomly and counted.

Xenograft assay

Parental or *OC2*-KD MKN01 cells (5×10^6 cells per mouse) were subcutaneously injected into nude mice (4–6 weeks old). Mice were monitored twice a week for tumor development. Tumor size was measured using Vernier calipers, and tumor volume was calculated according to the formula: volume = width^2 × length/2. Experiments followed the Laboratory Animals Act, Animal Protection Act and Institutional Animal Care and Use Committee (IACUC) guidelines and were approved according to institutional guidelines.

RNA-seq analysis

Total RNA from 1×10^7 control and *OC2*-expressing cells was extracted using the RNeasy Mini kit (Qiagen). An RNA sequencing library was prepared using the TruSeq RNA Sample Prep kit (Illumina), and sequencing was performed based on Nextseq500 platform (Illumina) to generate 75-bp paired-end reads. Sequenced reads were mapped to a human reference genome (hg19) using the STAR alignment tool (version 2.5.1),[12] and gene expression was quantified with the count module in STAR. The edgeR[13] package (version 3.12.1) was used to select differentially expressed genes based on the RNA-seq count data. The value for each gene (in counts per million) was normalized by trimmed mean of M values normalization, set to 1, and $\log_2$-transformed for further analysis.

RNA interference

To repress *ACSL5*, we used *ACSL5* small interfering RNAs (*ACSL5*-siRNAs 1,001,692 and 1,001,688, Bioneer, Daejeon, Korea). Corresponding scrambled sequences for each siRNA were also designed using the siRNA Wizard Software 3.1[14] and synthesized by Bioneer Company. For transfection, 2×10^5 MKN01 cells were plated in six-well plates and incubated overnight. MKN01 cells were transfected with siRNAs and scrambled RNAs (100 nM) using Lipofectamine RNAiMax (Invitrogen) in Opti-MEM medium (Thermo Fisher). After 24 hr incubation, the transfection medium was changed to complete medium. After 48 hr, KD was confirmed by qRT-PCR.

Statistical analysis

Details are provided in the Supporting Information.

Data availability

Gene expression and 450K HumanMethylation BeadChip data for 230 primary GCs,[15] including subtype EBV (24), CIN (111), GS (50) and MSI (45), and 450K HumanMethylation BeadChip data for two normal tissues were downloaded from The Cancer Genome Atlas (TCGA) portal (https://portal.gdc.cancer.gov/) and the National Center for Biotechnology Information (NCBI) Gene Expression Omnibus (GEO) (https://www.ncbi.nlm.nih.gov/geo/). Because the methylation data

from normal tissue is limited in TCGA database, we obtained additional data for 10 gastric mucosa (four from GSE50192 and six from GSE31848) from public databases[16,17] and used them produced by same platform without any selection process. CpG island (CGI) coordinates were obtained from the University of California, Santa Cruz (UCSC) browser. ChIP-seq and RNA-seq data for *OC2*-expressing cells are available from NCBI GEO (http://www.ncbi.nlm.nih.gov/geo/) *via* accession number GSE113045.

Results

OC2 is an early-onset hypomethylation target in GC development

Previously, we identified 174 hypomethylated differentially methylated promoters (DMPs) using methylome data from laser-capture microdissected GM, IM, and GC cells from a single patient with IGC.[5] These included 91 GC-specific and 83 early-onset DMPs. Early-onset hypomethylated DMPs indicate methylation differences of >twofold in IM and GC cells compared to GM. Of the 83 early-onset DMPs, 21 were noted for the high frequency of methylated reads compared to total reads in GM (Fig. 1*a*). Among these, *OC2* was a strong candidate for study of the development of GC, as the frequency of methylated reads to total reads was 0.66 in GM but only 0.02 and 0.05 in IM and GC, respectively (Fig. 1*a*). Again, UCSC Genome Browser (hg19) for RRBS data revealed that CpG methylation signatures (purple vertical lines in Fig. 1*c*) at promoter-proximal DNA of *OC2* was detected only in GM cells, but it was disappeared in IM or GC cells (Fig. 1*c*), indicating that promoter-proximal DNA of *OC2* was methylated in GM, but demethylated in IM or GC.

CpG hypomethylation at promoter-proximal DNA of *OC2* is associated with upregulation in primary gastric tumors

Bisulfite sequencing (see strategy in Fig. 1*d*) revealed that BS-R1 was methylation-free in all paired nontumors and tumors (left panels in Fig. 1*e*). On the other hand, in BS-R2 there were significant differences in methylation between nontumors and tumors (right panels in Fig. 1*e*), with average methylation approximately threefold higher in nontumors (37.71%) compared to tumors (12.21%). RT-PCR data revealed that *OC2* was silenced in nontumors but expressed in all tumors tested (Fig. 1*f*), suggesting that *OC2* expression in tumors may be associated with CpG hypomethylation at promoter-proximal DNA rather than the promoter region around the TSS.

From the RNA-seq and HumanMethylation 450K BeadChip public databases (see Public data section in Supporting Information), we acquired methylation data for 242 stomach tissue samples, including 12 nontumor samples and 230 tumor samples, which were divided into four molecular subtypes:[18] Epstein–Barr virus-positive (EBV), microsatellite instability (MSI), genomically stable (GS) and chromosomal instability (CIN). When we examined the CpG methylation level by the molecular subtype, we found that the greater variability in methylation on Exon 1 (BS-R2) in the tumor samples was due to variability in each subtype (Fig. 2*a*), indicating that the methylation on BS-R2 was heterogeneous depending on subtype of gastric tumors. For example, the methylation level at two CpG sites (cg02250594 and cg20324206) on BS-R2 was greatly increased in EBV subtype compared to that in normal, while in GS and MSI subtypes it was not much different to that in normal. On the other hand, the methylation level at the same CpG sites was clearly decreased in CIN subtype, which have mainly intestinal-type GC histology.[15] When we tested the correlation between *OC2* expression and methylation at four CpG sites on BS-R1 and BS-R2 in pooled tumors, the correlation coefficients ($r = -0.28$ for cg02250594 and $r = -0.29$ for cg20324206) for BS-R2 were much higher than those ($r = -0.17$ for cg15892115 and $r = -0.19$ for cg06275813) for BS-R1 (Fig. 2*b*). As it was tested at the same CpG sites only in CIN subtype tumors, the correlation coefficients for BS-R2 ($r = -0.21$ for cg02250594 and $r = -0.26$ for cg20324206) were much higher than those ($r = -0.07$ for cg15892115 and $r = -0.12$ for cg06275813) for BS-R1 (Fig. 2*c*). This results support the observation that CpG hypomethylation at promoter-proximal DNA of *OC2* is strongly associated with upregulation of *OC2* mRNA in gastric tumors, especially in CIN subtype.

We next quantified the extent of methylation at four CpG sites (CG#30–#33) including the above cg02250594 on BS-R2 by pyrosequencing (Fig. 1*d*) for 160 paired clinical tissues from the CNUH cohort and looked for a correlation with their qRT-PCR data. Pyrosequencing revealed that the mean percentage of methylation at these four sites was 28.8 ± 7.6% in nontumors and 18.1 ± 10.6% in tumors, indicating a significant decrease in methylation in tumor samples (Fig. 2*c*, $p < 2.2e{-}16$). qRT-PCR revealed that the mean percentage of *OC2* expression was 13.29 ± 5.49% in nontumors and 16.70 ± 3.60% in tumors, indicating significant upregulation of *OC2* in tumors compared to nontumors (Fig. 2*d*, $p = 2.848e{-}09$). An increase in *OC2* expression was detected in 64% (102/160) of tumors, for which an increase in expression was defined as a >twofold increase in the values for tumors compared to paired nontumors. Additionally, there was a negative correlation between methylation at the four CpG sites and *OC2* expression in tumors (Fig. 2*e*, $r = -0.23$, $p = 4e{-}03$).

OC2 is expressed in IM as well as GC

We performed immunohistochemistry with anti-*OC2* to compare the amount of *OC2* in nontumor, IM and GC tissues. The data revealed strong staining for *OC2* in the nucleus but weak staining in the cytoplasm of goblet cells of IMs (Figs. 3*b*, 3*f* and 3*j*) and IGCs (Figs. 3*c*, 3*g* and 3*k*), but *OC2* was not detectable in paired normal tissue (Figs. 3*a*, 3*e* and 3*i*). In addition, there is no staining in diffuse-type GCs (DGCs; Figs. 3*n* and 3*p*) or paired normal tissue (Figs. 3*m* and 3*o*). These results indicated that *OC2* expression was repressed in normal cells but induced in IM and IGC cells, suggesting that *OC2* may be associated with early development of IGC.

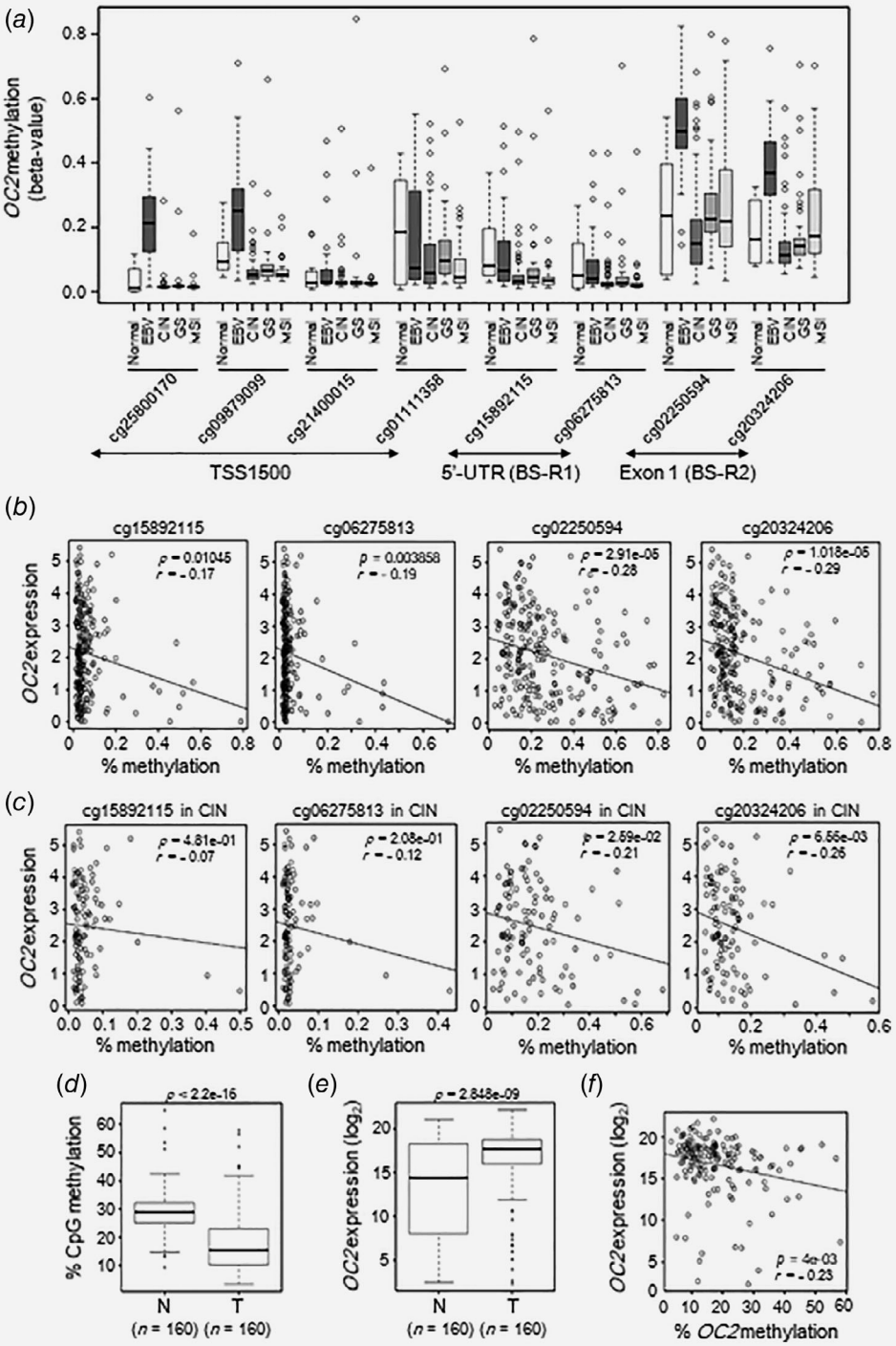

Figure 2. Association between *OC2* methylation and expression in primary gastric tumors. (*a*) Methylation status at CpG sites around the *OC2* promoter region. Beta-values at eight CpG sites from TSS1500, the 5′-untranslated region (5′-UTR), and exon 1 were retrieved from HumanMethylation 450K data for 12 gastric mucosa and 230 gastric tumors including subtype EBV (24), CIN (111), GS (50) and MSI (45) from the TCGA database. TSS1500, 200–1,500 bases upstream of the TSS. (*b*) Correlation of *OC2* expression with CpG methylation in pooled gastric tumors. RNA-seq data from TCGA was plotted graphically with beta-values at four CpGs (cg15892115 and cg06275831 from BS-R1; cg02250595 and cg20324206 from BS-R2). (*c*) Correlation of *OC2* expression with CpG methylation in CIN subtype tumors. It was performed at the same CpG positions in Figure 2*b*. (*d*) *OC2* methylation in 160 paired nontumor tissues and gastric tumors from the CNUH cohort. Pyrosequencing was performed at the four CpG sites shown in Figure 1*d*. The average value of methylation was estimated for each sample. (*e*) *OC2* expression in the same paired samples from the CNUH cohort. qRT-PCR was performed and expression was normalized to *β-actin* expression in each sample. (*f*) Pearson's correlation analysis between *OC2* methylation and expression in the CNUH cohort. Box plot analyses in panels *a*, *c* and *d* show median, 25th and 75th percentiles and outliers.

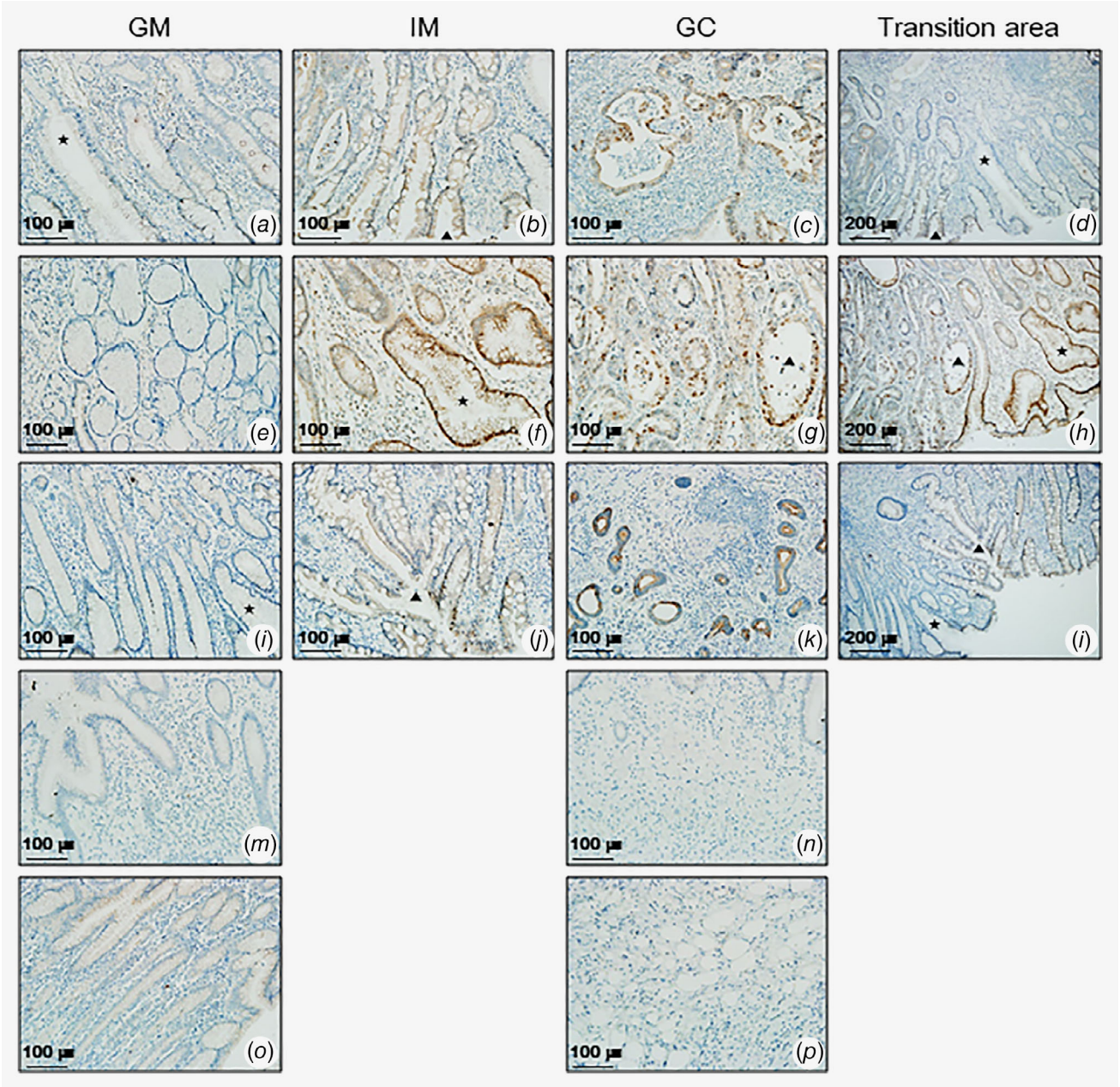

Figure 3. Immunohistochemical staining for *OC2* in paired clinical tissues from five patients. *OC2* was examined in formalin-fixed, paraffin-embedded sections from two types of GC using rabbit anti-*OC2*. The top three rows (*a–l*) represent IGC tissues three patients, the bottom two rows (*m–p*) represent DGC tissues from two patients. Left three panels from each row show GM, IM and GC lesions and the far right panel show transition areas between GM and IM (*d*, *a* + *b*), between IM and GC (*h*, *f* + *g*), and between GM and IM (*l*, *i* + *j*). Filled star and triangle indicate same position between images of each lesion and transition area. The bottom two rows (*m–p*) represent DGC tissues showing only GM and GC lesions. All images were acquired at 100× or 200× magnification.

Bivalent chromatin domain is associated with *OC2* repression in GC cell lines

We performed RT-PCR and bisulfite sequencing with GC cell lines in the same manner as in Figure 2. We also performed Western blot analysis to explore whether *OC2* mRNA expression level correlates with its protein expression or not. The RT-PCR and Western blot results revealed that the mRNA expression and protein expression varied among the 16 GC cell lines (Fig. 4*a*). Then we found that *OC2* mRNA expression and protein expression levels were inconsistent with each other in some GC cell lines, such as SNU001, SNU016, SNU620, SNU638, AGS and MKN74, as shown in Figure 4*a*. For convenience, the 16 GC cell lines were divided into two groups based on *OC2* protein expression (expressed or silenced), eight of these GC cell lines, which represent each group, were selected at random (Fig. 4*b*), and used to examine

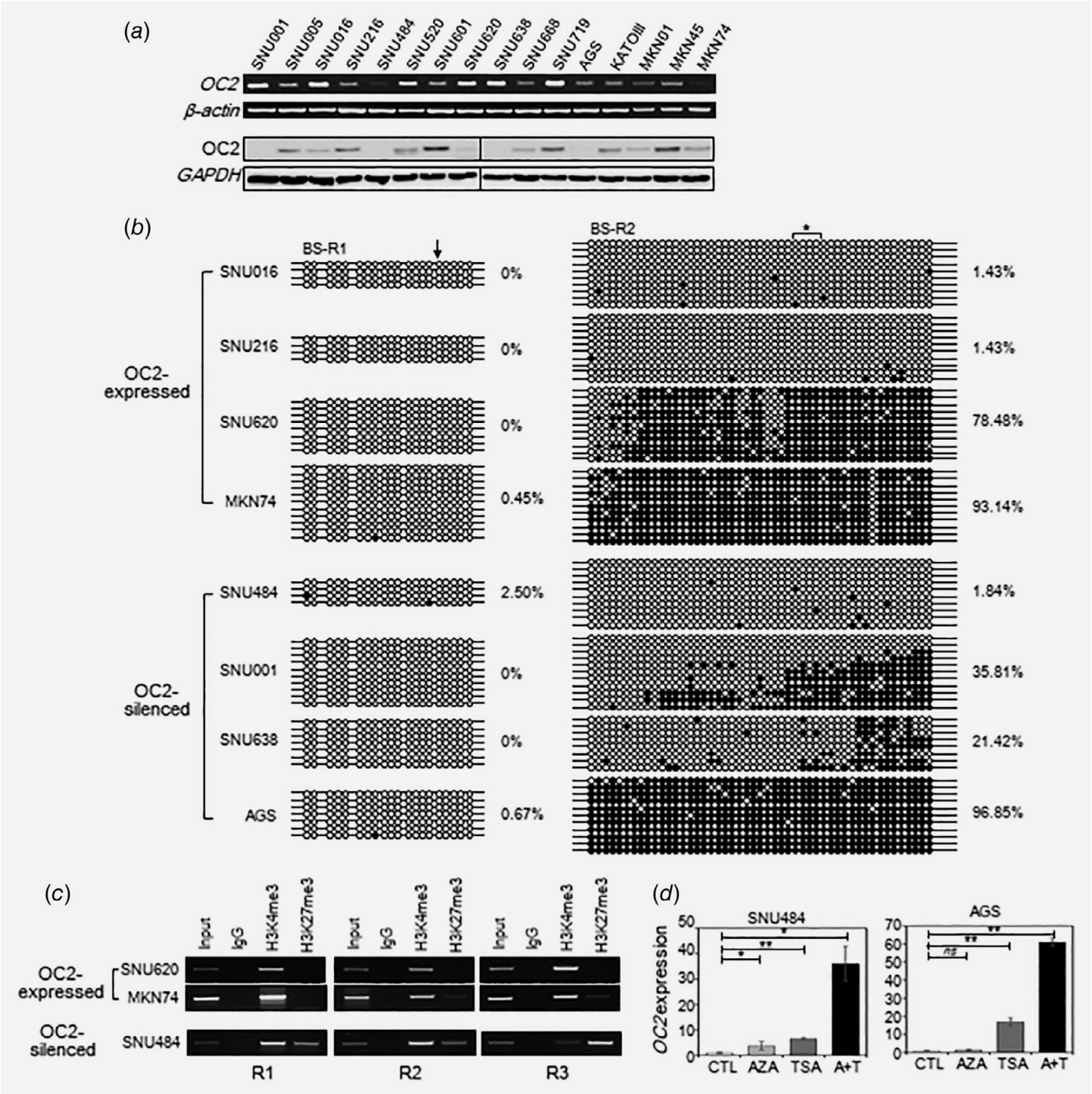

Figure 4. *OC2* Expression, bisulfite sequencing and ChIP-PCR in GC cell lines. (*a*) RT-PCR results for 16 GC cell lines. (*b*) Eight GC cell lines were categorized based on level of *OC2* expression as assessed with RT-PCR (4 Strong, 2 Weak and 2 Silenced). Bisulfite sequencing was performed as in Figure 1*e*. (*c*) ChIP at the three regions in Figure 1*d* for eight lines categorized as strong or weak/silenced. H3K4me3 and H3K27me3 were used as active and repressed markers, respectively. IgG was used as a negative control. (*d*) Restoration of *OC2* mRNA level after treatment with 5-aza-dC (AZA) and/or trichostatin A (TSA). *OC2* expression was examined by qRT-PCR and normalized to *β-actin* expression in each sample. Each value is the mean ± SD of three independent experiments. **p* ‹ 0.05, ***p* ‹ 0.01 *versus* untreated (CTL) cells; *ns*: nonsignificant.

the correlation between expression and methylation at BS-R1 or BS-R2. Bisulfite sequencing revealed that all CpG sites at BS-R1 in all groups were not methylated (left panels in Fig. 4*b*), similar to clinical tissues (left panels in Fig. 1*e*). On the other hand, the extent of BS-R2 methylation depended on the *OC2* expression group (right panels in Fig. 4*b*). In the *OC2*-expressed group, SNU016 and SNU216 were almost methylation free (both, 1.43%), while SNU620 and MKN74 had heavy methylation at 78.48 and 93.14%. The *OC2*-silenced group. In the *OC2*-silenced group, SNU001, SNU638 and AGS had methylation ranging 21.42–96.85%, while SNU484 was almost methylation free (1.84%). Thus, we observed

negative correlation between *OC2* expression and BS-R2 methylation in SNU016, SNU216, SNU001, SNU638 and AGS, but unusual pattern in SNU620, MKN74 and SNU484.

To characterize histone marks associated with chromatin remodeling in GC cell lines with unusual pattern, we performed ChIP-PCR at the three regions shown in Figure 1*d*. The SNU620 and MKN74, in which *OC2* expressed but had heavy BS-R2 methylation, showed only H3K4me3 signatures (an active mark) at the three regions Ch-R1, Ch-R2 and Ch-R3 (upper panels in Fig. 4*c*). On the other hand, the SNU484, in which *OC2* silenced but had almost BS-R2 methylation-free, showed bivalent marks of H3K4me3 and H3K27me3 at the three regions (lower panels in Fig. 4*c*), suggesting that the bivalent marks may be indicative of an association with *OC2* silencing. To determine whether *OC2* expression is controlled epigenetically, we treated cells with the DNA methylation inhibitor 5-aza-dC and/or the histone deacetylase inhibitor trichostatin A. After treatment with either drug, *OC2* expression was restored compared to untreated cells (Fig. 4*d*), indicating that *OC2* expression is regulated by epigenetic mechanisms, including DNA methylation and/or histone modification.

OC2 has oncogenic potential *in vitro*

We next examined the effect of ectopic *OC2* expression in MKN74 or AGS cells, in which *OC2* was repressed or weakly expressed (Fig. 4*a*). Western blotting and qRT-PCR confirmed that *OC2* was stably expressed in *OC2*-transfected MKN74 (*OC2*-MKN74) and AGS (*OC2*-AGS) cells (Fig. 5*a*). Colony-forming assays revealed that *OC2* significantly induced colony formation in each of *OC2*-MKN74 and *OC2*-AGS cells (Fig. 5*b*). *OC2* also significantly induced cell migration in both *OC2*-transfected lines (Fig. 5*c*), invasion in *OC2*-MKN74 cells (Fig. 5*d*) and cell proliferation in both lines (Fig. 5*e*).

shRNA targeting of *OC2* modulates oncogenic properties *in vitro* and *in vivo*

We examined whether *OC2* expression in SNU216 or MKN01 cells could be knocked down by treatment of with one or two different shRNAs (Fig. 4*a*). Western blotting and qRT-PCR confirmed that *OC2* expression was significantly decreased in *OC2*-KD SNU216 and MKN01 cells after treatment with either of the two shRNAs (Fig. 5*f*). Both shRNAs significantly decreased colony formation and cell proliferation in both *OC2*-KD cell lines compared to control shRNA (Fig. 5*g*). One shRNA (sh#4) also significantly decreased the migration and invasion capacities of both *OC2*-KD lines, whereas the other shRNA (sh#3) decreased migration and invasion only in MKN01 cells (Figs. 5*h* and 5*i*). These results indicated that shRNAs targeting *OC2* mRNA could modulate the oncogenic potential of *OC2*. In addition, we examined the loss of function using *OC2*-siRNAs in ectopic *OC2* expression cells (*OC2*-AGS). The result showed that *OC2* was efficiently and specifically reduced in *OC2*-AGS cells by *OC2*-specific siRNAs compared to cells treated with the scrambled siRNAs (Supporting Information Fig. S4*a*) and that potential of colony-forming (Supporting Information Fig. S4*b*) and migration (Supporting Information Fig. S4*c*) were significantly reduced in *OC2*-AGS cells by *OC2* knockdown. Finally, an *in vivo* study revealed that tumors in mice xenografted with *OC2*-KD cells were significantly smaller than those of mice xenografted with empty-vector cells (Fig. 5*k*), demonstrating that tumorigenicity could be suppressed by shRNA targeting *OC2* mRNA.

OC2 triggers *ACSL5* in GC cells

To further investigate the functional role of *OC2* as a transcription factor, we performed ChIP-seq and RNA-seq analysis of *OC2*-AGS and *OC2*-MKN74 cells. ChIP-seq analysis using Homer revealed that the consensus motif with the highest enrichment of a single *OC2*-binding site was *HNF6* (5′-ATC/TGAT-3′) in both cell lines and controls. That is, 76.51% (9,336) and 38.08% (652) of total *OC2* peaks in *OC2*-AGS and control (Supporting Information Fig. S1*a*) were significantly matched to the *HNF6* motif (p = 1e−7,601 and 1e−50, left panel in Fig. 6*a*). In *OC2*-MKN74 and control, 73.45% (74,543) and 52.02% (3,023) of total *OC2* peaks (Supporting Information Fig. S1*b*) were significantly matched to the *HNF6* motif (p = 1e−54,622 and 1e−1,678, right panel in Fig. 6*a*). We then focused on *OC2* peaks at the *HNF6* motif in only the promoter region (±1 kb of TSS), revealing a significant increase in *OC2* peaks throughout the course of transfection of cells with *OC2*: 224 peaks in *OC2*-AGC cells (Supporting Information Fig. S1*c* and Table S3) and 1,353 peaks in *OC2*-MKN74 cells (Supporting Information Fig. S1*d*; Supplementary Table S4) were significantly increased ≥fourfold compared to each control ($p < 0.0001$). Finally, there were 198 *OC2* peaks in common between the 224 *OC2*-AGS peaks and the 1,353 *OC2*-MKN74 peaks (yellow circle in Fig. 6*b*).

RNA-seq analysis showed that 507 genes, of which only 6 had common *OC2* peaks at each promoter, were upregulated ≥twofold in *OC2*-AGS cells compared to control (red circle in Fig. 6*b*; Supporting Information Table S5). For *OC2*-MKN74 cells, 414 genes, of which only five had common *OC2* peaks at each promoter, were upregulated ≥twofold compared to control (blue circle in Fig. 6*b*; Supporting Information Table S6).

Finally, we identified two genes, namely, *ACSL5* and *complement factor B* (*CFB*), which were upregulated and had *OC2* peaks at the promoter in *OC2*-AGS and *OC2*-MKN74 cells (Fig. 6*b*). Using the Gene Expression across Normal and Tumor tissue (GENT) database,[19] we confirmed a positive correlation between the expression of *OC2* and *ACSL5* (r = 0.29, left in Fig. 6*c*) and between *OC2* and *CFB* (r = 0.18, right in Fig. 6*c*) in 311 gastric tumor tissues. Using the UCSC Genome Browser, we found significant increases of *OC2* peaks at the promoter region of *ACSL5* and induction of *ACSL5* expression in *OC2*-AGS or *OC2*-MKN74 cells (Fig. 6*d*). The induction of *ACSL5* expression was confirmed in both *OC2*-AGS and *OC2*-MKN74 cells, as assessed with qRT-PCR (Fig. 6*e*). To determine whether *OC2* is an

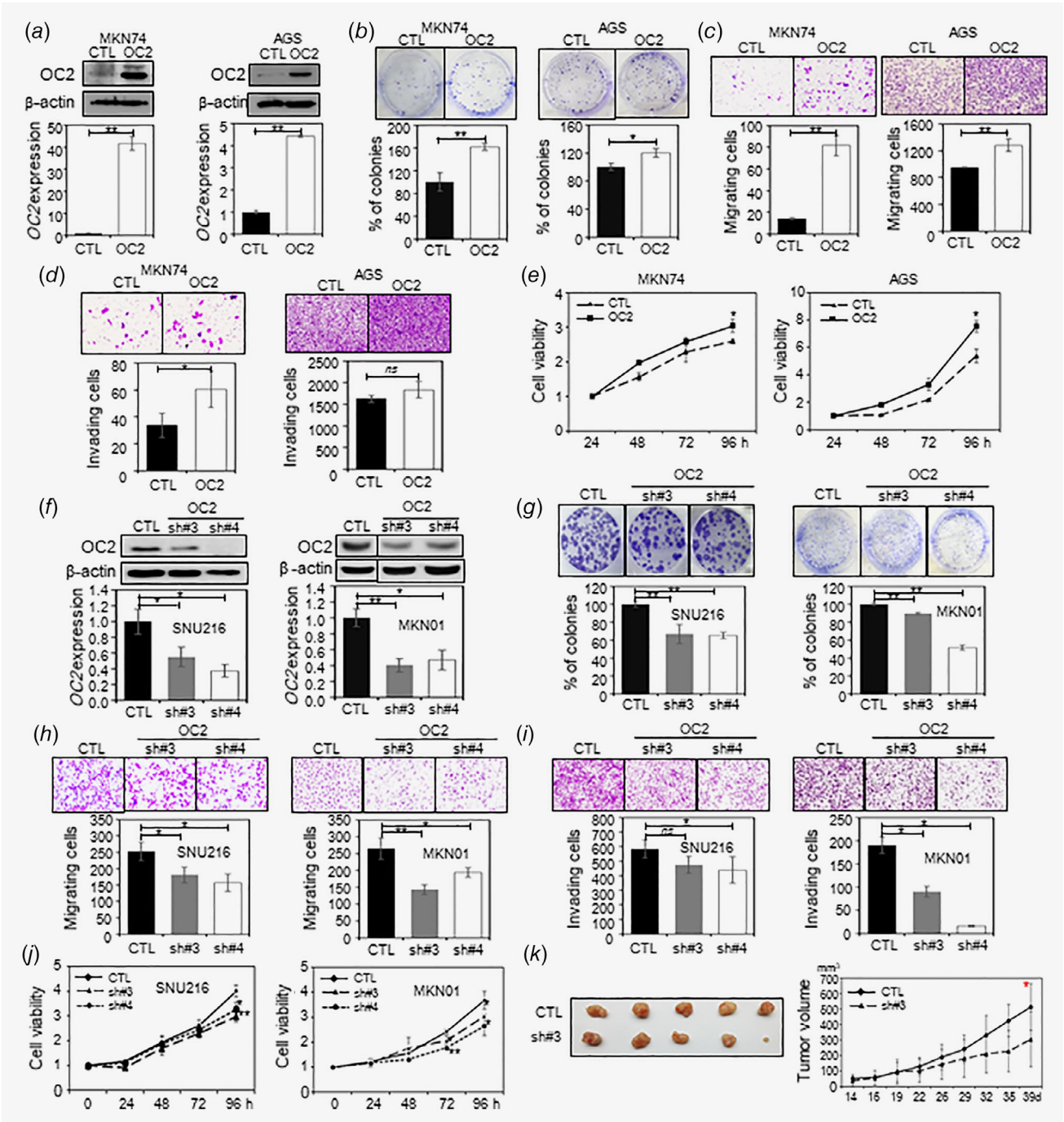

Figure 5. *In vitro* and *in vivo* assays of ectopic *OC2* expression or *OC2* KD. (*a*) Establishment of *OC2*-expressing cells. The GC cell lines MKN74 (left) and AGS (right) were transfected with a lentiviral *OC2* expression vector. *OC2* expression was compared to that measured for cells transfected with an empty vector control (CTL) as assessed with western blotting (top) and qRT-PCR (bottom). β-actin was used as an internal control. (*b*) Colony formation assay. Transfected cells were plated on six-well plates at 5×10^2 cells per well. After 2 weeks, colonies were stained with crystal violet and counted. (*c*) Migration assay. Transfected cells were plated on transwell chambers at 2×10^4 cells per well. After 18–22 hr, transwell membranes were stained with crystal violet and cells were counted. (*d*) Invasion assay. Transfected cells were plated on Matrigel-coated transwell chambers at 2×10^4 cells per well. After 22–24 hr, transwell membranes were stained with crystal violet and cells were counted. (*e*) Proliferation assay. Relative proliferation of *OC2*-expressing cells over 4 days was measured using a CCK-8 kit and compared to the empty vector control. (*f*) Establishment of *OC2*-KD cells by shRNA. SNU216 (left) and MKN01 (right) cells were transfected with two lentiviral *OC2* shRNAs (sh#3 and sh#4), and cells were then cultured for 2 weeks. KD cells were compared to cells transfected with shRNA control *via* western blotting (top) and qRT-PCR (bottom). β-actin was used as an internal control. (*g–j*) Colony formation, migration, invasion and proliferation assays were performed as above. For proliferation assays, KD cells were compared to cells transfected with control shRNA. (*k*) *In vivo* assay using grafts from transfected SNU216 cells. Left: Tumors excised 39 days after injection of stably transfected *OC2*-KD cells *versus* control cells into nude mice. Right: Graph of calculated tumor volume *versus* days after injection.

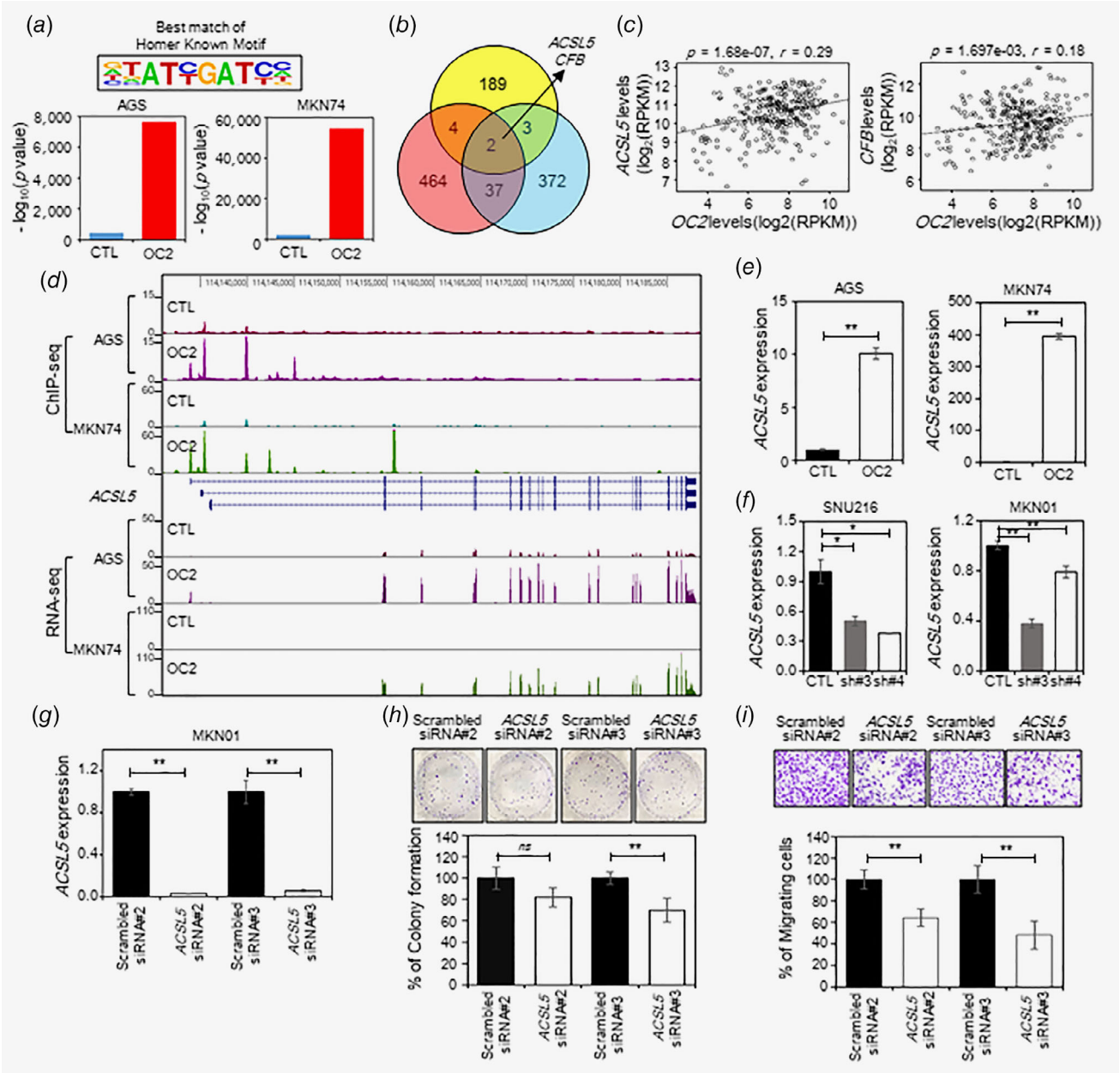

Figure 6. ChIP-seq and RNA-seq analysis of GC cells with ectopic *OC2* expression. (*a*) Consensus motif with the highest enrichment of *OC2*-binding sites as assessed with ChIP-seq. The consensus motif was derived from binding sequences of *OC2*-MKN74 and *OC2*-AGS cells using Homer software. (*b*) Intersection of *OC2*-binding and upregulated genes in *OC2*-AGS and *OC2*-MKN74 cells. Yellow circle: 198 *OC2* peaks at promoter regions detected in both *OC2*-transfected cell lines; red and blue circles: 507 and 414 genes upregulated twofold in *OC2*-MKN74 and *OC2*-AGS cells, respectively. The intersection of all three circles yielded only two genes, namely *ACSL5* and *CFB*, as targets induced by *OC2* in both cell lines. (*c*) Correlation of expression levels between *OC2* and either *ACSL5* (left) or *CFB* (right) in 311 gastric tumor tissues from the GENT database. (*d*) UCSC Genome Browser view of ChIP-seq and RNA-seq data for *ACSL5* at human chromosome 10q25.2 in both *OC2*-transfected cell lines showing *OC2* peak enrichment at the *ACSL5* promoter and induction of *ACSL5* transcription in both *OC2*-transfected cell lines. (*e*) Confirmation of *ACSL5* induction in *OC2*-AGS and *OC2*-MKN74 cells by qRT-PCR. (*f*) Confirmation of *ACSL5* reduction in *OC2*-KD SNU216 and MKN01 cells by qRT-PCR. (*g*) KD of *ACSL5* by siRNA. MKN01 cells were transfected with *ACSL5*-specific or control siRNA, and *ACSL5* mRNA level was examined by qRT-PCR. (*h*, *i*) Colony formation and migration assays for *ACSL5*-KD MKN01 cells. All assays were performed as described in Figure 6. siRNA KD cells were compared to cells transfected with scrambled siRNA.

upstream regulator of *ACSL5*, we examined *ACSL5* expression in each of *OC2*-KD SNU216 and *OC2*-KD MKN01 cells (Fig. 5*f*). qRT-PCR revealed significantly decreased *ACSL5* expression in *OC2*-KD SNU216 and *OC2*-KD MKN01 cells compared to control cells (Fig. 6*f*), suggesting that *ACSL5* expression is dependent on *OC2* activity.

Repression of *ACSL5* by siRNA inhibits GC oncogenic properties *in vitro*

To test the oncogenic potential of *ACSL5 in vitro* irrespective of *OC2*-KD, we transfected MKN01 cells with two individual siRNAs targeting RNA sequences of *ACSL5* (in those cells, *ACSL5* expression had been induced; see Supporting Information Fig. S2). qRT-PCR confirmed that *ACSL5* expression was significantly decreased in *ACSL5*-KD MKN01 cells after treatment with either of the siRNAs (Fig. 6*g*). siRNA#3 significantly decreased the colony-forming potential of *ACSL5*-KD MKN01 cells compared to scrambled siRNAs (Fig. 6*h*). In addition, each of the siRNAs caused a decrease in the migration (Fig. 6*i*) of *ACSL5*-KD MKN01 cells compared to cells treated with the scrambled siRNAs. These results demonstrated that siRNA-mediated repression of *ACSL5* inhibits the oncogenicity of MKN01 cells.

Discussion

In our study, we demonstrated that CpG sites in the promoter region of *OC2* were unmethylated in gastric tumors as well as nontumor cells but that regional CpG sites in *OC2* exon 1 were aberrantly hypomethylated in tumors and that *OC2* was also aberrantly upregulated in tumors. Notably, DNA hypomethylation occurred in IM as well as IGC, suggesting that *OC2* expression may be induced during the precancer IM stage. Furthermore, we observed anti-*OC2* staining in IM as well as IGC, but not in normal mucosa or DGC. *OC2* promoted GC cell proliferation and tumor growth *in vitro* and *in vivo*. To the best of our knowledge, our results are the first to indicate that regional CpG hypomethylation at *OC2* exon 1 contributes to tumorigenesis as an early event in IGC development and that inhibition of this hypomethylation constitutes a potential therapeutic target for IGC.

To describe the relationship between promoter-proximal DNA methylation and transcriptional efficiency, a model has been proposed with four alternative DNA methylation states.[20] First, methylation of the promoter region itself leads to robust silencing of the gene, as is frequently observed for CpG island promoters in cancer cells. Second, promoter-proximal methylation (~300 bp from the TSS) may have a dramatic effect on transcription initiation, as a result of altering chromatin structure at the promoter. Third, heavy DNA methylation within ~1 kb from the TSS may have a modest effect on transcription elongation efficiency, perhaps by altering the chromatin structure of the promoter-proximal region. Fourth, in the presence of distal DNA methylation (1–2 kb from the TSS), transcription may not be affected. We found that the promoter region of *OC2* was completely unmethylated in all nontumor tissues and tumors, regardless of *OC2* transcription level, suggesting that the promoter region (BS-R1, −117 to +41 bp from TSS) may not be critical for regulating *OC2* transcription. Among the above model, the second methylation state appears to reflect a more probable model for how *OC2* transcription is regulated because CpG hypomethylation at the promoter-proximal DNA of *OC2* (BS-R2, +209 to +685 bp from TSS) was associated with *OC2* transcription in tumors.

Similarly, the *OC2* promoter region in GC cell lines may not be critical for regulating transcription because, again, the promoter region was methylation-free in all GC cell lines. However, the relationship between promoter-proximal DNA methylation and transcriptional efficiency in the cell lines tested is less clear. For example, SNU620 cells had heavy methylation at *OC2* promoter-proximal region and expressed *OC2* strongly, whereas SNU216 and SNU484 cells were methylation-free at the *OC2* promoter-proximal region and expressed *OC2* weakly or not at all. Thus, our data cannot explain the relationship between *OC2* promoter-proximal DNA methylation and *OC2* transcription in GC cells. In the promoter-proximal regions, on the other hand, we observed an H3K4me3 mark in GC cell lines with strong *OC2* expression, but there was a bivalent H3K4me3/H3K27me3 mark in GC cell lines with weak or no *OC2* expression. This result corresponds well with previous reports that such bivalent marks lead to transcriptional silencing and are common in adult tumor cells.[20,21] It is not known how heavy methylation at the *OC2* promoter-proximal DNA is associated with the H3K4me3 mark in SNU620, or whether methylation-free promoter-proximal DNA is associated with the bivalent mark H3K4me3/H3K27me3 in SNU216 or SNU484 cells. Further investigation is required to elucidate the unusual relationship between *OC2* promoter-proximal DNA methylation and chromatin structure.

The ONECUT transcription factors, including *OC2*, are evolutionarily conserved proteins that play a role in the development of the liver, pancreas and neuronal system.[22–24] Although a role for *OC2* in cancer is not well defined, it was recently reported that *OC2* was aberrantly upregulated in a variety of cancer types, including hepatocellular carcinoma, prostate cancer, colorectal cancer and ovarian cancer.[7,25–27] Recently, it has been proposed that during the multistep development human tumors acquire six hallmarks of cancer, including sustaining proliferative signaling, evading growth suppressors, resisting cell death, enabling replicative immortality, inducing angiogenesis and activating invasion and metastasis.[28] The conceptual progress has added two emerging hallmarks of reprogramming of energy metabolism and evading immune destruction to the list.[29] As underlying these hallmarks, genome instability and inflammation has been suggested.[29] In recent years, it has been suggested that specific shifts in chromatin configuration could occur during the acquisition of certain hallmark capabilities.[30] In our study, we demonstrated that *OC2* acquired aberrant gain of function in GC as a consequence of specific epigenetic alterations and promoted GC cell proliferation and tumor growth *in vitro* and *in vivo*, thus suggesting that *OC2* plays an important role during the acquisition of some hallmark capabilities in a variety of human cancers including GC. In addition, *OC2* mRNA

is a urine biomarker for the detection of PC,[26] and a risk-associated genetic variant in prostate cancer patients has been associated with *OC2* activity,[31] and *OC2* acts as a master regulator and survival factor in aggressive prostate cancer variants.[8] Moreover, *OC2* is also a target for the microRNA miR-429 or miR-9, downregulation of which is associated with *OC2* activation, which may contribute to the development of hepatocellular carcinoma[25] or colorectal cancer.[7]

Gastric carcinogenesis proceeds through a series of precursor lesions in the GM called Correa's cascade, comprised of multi-atrophic gastritis, IM, dysplasia and finally GC.[32] In this process, IM is a trans-differentiation of the gastric epithelium to yield an intestinal type, mostly induced by *Helicobacter pylori* infection and expression of homeobox genes, including *caudal type homeobox 2* (*CDX2*).[33] There is emerging epidemiological evidence that IM may be reversible with long-term follow up. For instance, a recent study showed that *H. pylori* eradication may reverse IM at least in a subset of patients and that reversibility may be associated with a decrease in *CDX2* mRNA in patients with dysplasia as well as GC.[34] However, the results of earlier studies on the effects of *H. pylori* eradication for improving IM have been inconsistent.[35–38] Another recent study reported that selumetinib, an inhibitor of mitogen-activated protein kinase, might reverse IM in a mouse model based on tamoxifen injection and lead to re-establishment of normal gastric lineages.[39] Interestingly, in the normal gastrointestinal tract, ACSL5 in the small intestine is predominantly found in the villus epithelium and not in the GM, whereas in the stomach high levels of ACSL5 are found in the IM, suggesting that ACSL5 may play an important role in the progression of IM[40] and may be a target for reversing IM in the stomach. If *ACSL5* is a downstream target of *OC2*, as shown in our present study, one would expect that its activity can be inhibited by modulation of *OC2*. In a mouse model of metastatic prostate cancer, *OC2* was shown to be inhibited by CSRM617, a newly identified small molecule.[8] Additionally, we confirmed a positive correlation between *CDX2*, *OC2* and *ACSL5* expression in 311 gastric tumor tissues (Supporting Information Fig. S3), suggesting that three IM markers may be associated with intestinal differentiation or development of IGC.

Taken together, our data indicate that *OC2* is a novel IM marker that is hypomethylated longitudinally in IGC and its precancer lesion, IM. Further, we propose that *OC2* and its downstream target *ACSL5* could be used to develop early detection biomarkers and to prevent gastric carcinogenesis. Our findings contribute to the Pre-Cancer Genome Atlas (PCGA), a concerted initiative to characterize the molecular alterations in premalignant lesions.[41] Further studies are required to clarify the exact role of *ACSL5* in gastric carcinogenesis and to evaluate whether small molecules such as CSRM617 can modulate *OC2* and thus *ACLS5*.

Acknowledgements

This work was supported by a National Research Foundation of Korea (NRF) grant funded by the Korean government (no. 2017R1E1A1A01074883) and a Korea Research Institute of Bioscience and Biotechnology (KRIBB) Research Initiative grant.

Conflict of interest

The authors declare that they have no conflict of interest.

References

1. Ferlay J, Shin HR, Bray F, et al. Estimates of worldwide burden of cancer in 2008: GLOBOCAN 2008. *Int J Cancer* 2010;127: 2893–917.
2. Jones PA, Baylin SB. The fundamental role of epigenetic events in cancer. *Nat Rev Genet* 2002;3: 415–28.
3. Szyf M, Pakneshan P, Rabbani SA. DNA methylation and breast cancer. *Biochem Pharmacol* 2004; 68:1187–97.
4. Upchurch GM, Haney SL, Opavsky R. Aberrant promoter Hypomethylation in CLL: does it matter for disease development? *Front Oncol* 2016;6:182.
5. Kim HJ, Kang TW, Haam K, et al. Whole genome MBD-seq and RRBS analyses reveal that hypermethylation of gastrointestinal hormone receptors is associated with gastric carcinogenesis. *Exp Mol Med* 2018;50:156.
6. Hodge LK, Klassen MP, Han BX, et al. Retrograde BMP signaling regulates trigeminal sensory neuron identities and the formation of precise face maps. *Neuron* 2007;55:572–86.
7. Sun Y, Shen S, Liu X, et al. MiR-429 inhibits cells growth and invasion and regulates EMT-related marker genes by targeting Onecut2 in colorectal carcinoma. *Mol Cell Biochem* 2014;390:19–30.
8. Rotinen M, You S, Yang J, et al. ONECUT2 is a targetable master regulator of lethal prostate cancer that suppresses the androgen axis. *Nat Med* 2018;24:1887–98.
9. Kim M, Kim JH, Jang HR, et al. LRRC3B, encoding a leucine-rich repeat-containing protein, is a putative tumor suppressor gene in gastric cancer. *Cancer Res* 2008;68:7147–55.
10. Langmead B, Salzberg SL. Fast gapped-read alignment with bowtie 2. *Nat Methods* 2012;9:357–9.
11. Heinz S, Benner C, Spann N, et al. Simple combinations of lineage-determining transcription factors prime cis-regulatory elements required for macrophage and B cell identities. *Mol Cell* 2010; 38:576–89.
12. Dobin A, Davis CA, Schlesinger F, et al. STAR: ultrafast universal RNA-seq aligner. *Bioinformatics* 2013;29:15–21.
13. McCarthy DJ, Chen Y, Smyth GK. Differential expression analysis of multifactor RNA-Seq experiments with respect to biological variation. *Nucleic Acids Res* 2012;40:4288–97.
14. Fakhr E, Zare F, Teimoori-Toolabi L. Precise and efficient siRNA design: a key point in competent gene silencing. *Cancer Gene Ther* 2016;23:73–82.
15. The Cancer Genome Atlas Research Network. Comprehensive molecular characterization of gastric adenocarcinoma. *Nature* 2014;513:202–9.
16. Lokk K, Modhukur V, Rajashekar B, et al. DNA methylome profiling of human tissues identifies global and tissue-specific methylation patterns. *Genome Biol* 2014;15:r54.
17. Nazor KL, Altun G, Lynch C, et al. Recurrent variations in DNA methylation in human pluripotent stem cells and their differentiated derivatives. *Cell Stem Cell* 2012;10:620–34.
18. Cancer Genome Atlas Research Network. Comprehensive molecular characterization of gastric adenocarcinoma. *Nature* 2014;513:202–9.
19. Shin G, Kang TW, Yang S, et al. GENT: gene expression database of normal and tumor tissues. *Cancer Inform* 2011;10:149–57.
20. McGarvey KM, Van Neste L, Cope L, et al. Defining a chromatin pattern that characterizes DNA-hypermethylated genes in colon cancer cells. *Cancer Res* 2008;68:5753–9.
21. Rodriguez J, Munoz M, Vives L, et al. Bivalent domains enforce transcriptional memory of DNA methylated genes in cancer cells. *Proc Natl Acad Sci USA* 2008;105:19809–14.
22. Espana A, Clotman F. Onecut factors control development of the locus Coeruleus and of the mesencephalic trigeminal nucleus. *Mol Cell Neurosci* 2012;50:93–102.
23. Jacquemin P, Lannoy VJ, Rousseau GG, et al. OC-2, a novel mammalian member of the ONECUT class of homeodomain transcription factors whose function in liver partially overlaps

with that of hepatocyte nuclear factor-6. *J Biol Chem* 1999;274:2665–71.
24. Vanhorenbeeck V, Jenny M, Cornut JF, et al. Role of the Onecut transcription factors in pancreas morphogenesis and in pancreatic and enteric endocrine differentiation. *Dev Biol* 2007;305:685–94.
25. Zhang J, Cheng J, Zeng Z, et al. Comprehensive profiling of novel microRNA-9 targets and a tumor suppressor role of microRNA-9 via targeting IGF2BP1 in hepatocellular carcinoma. *Oncotarget* 2015;6:42040–52.
26. Leyten GH, Hessels D, Smit FP, et al. Identification of a candidate gene panel for the early diagnosis of prostate cancer. *Clin Cancer Res* 2015;21:3061–70.
27. Lu T, Wu B, Yu Y, et al. Blockade of ONECUT2 expression in ovarian cancer inhibited tumor cell proliferation, migration, invasion and angiogenesis. *Cancer Sci* 2018;109:2221–34.
28. Hanahan D, Weinberg RA. The hallmarks of cancer. *Cell* 2000;100:57–70.
29. Hanahan D, Weinberg RA. Hallmarks of cancer: the next generation. *Cell* 2011;144:646–74.
30. Berdasco M, Esteller M. Aberrant epigenetic landscape in cancer: how cellular identity goes awry. *Dev Cell* 2010;19:698–711.
31. Guo H, Ahmed M, Zhang F, et al. Modulation of long noncoding RNAs by risk SNPs underlying genetic predispositions to prostate cancer. *Nat Genet* 2016;48:1142–50.
32. Correa P, Piazuelo MB. The gastric precancerous cascade. *J Dig Dis* 2012;13:2–9.
33. Mesquita P, Raquel A, Nuno L, et al. Metaplasia—a transdifferentiation process that facilitates cancer development: the model of gastric intestinal metaplasia. *Crit Rev Oncog* 2006;12:3–26.
34. Shin CM, Kim N, Chang H, et al. Follow-up study on CDX1 and CDX2 mRNA expression in noncancerous gastric mucosae after helicobacter pylori eradication. *Dig Dis Sci* 2016;61:1051–9.
35. Tucci A, Poli L, Tosetti C, et al. Reversal of fundic atrophy after eradication of helicobacter pylori. *Am J Gastroenterol* 1998;93:1425–31.
36. Sung JJ, Lin SR, Ching JY, et al. Atrophy and intestinal metaplasia one year after cure of H. pylori infection: a prospective, randomized study. *Gastroenterology* 2000;119:7–14.
37. Ohkusa T, Fujiki K, Takashimizu I, et al. Improvement in atrophic gastritis and intestinal metaplasia in patients in whom helicobacter pylori was eradicated. *Ann Intern Med* 2001;134:380–6.
38. Kang JM, Kim N, Shin CM, et al. Predictive factors for improvement of atrophic gastritis and intestinal metaplasia after helicobacter pylori eradication: a three-year follow-up study in Korea. *Helicobacter* 2012;17:86–95.
39. Choi E, Hendley AM, Bailey JM, et al. Expression of activated Ras in gastric chief cells of mice leads to the full Spectrum of metaplastic lineage transitions. *Gastroenterology* 2016;150:918–30. e13.
40. Gassler N, Obermuller N, Keith M, et al. Characterization of metaplastic and heterotopic epithelia in the human gastrointestinal tract by the expression pattern of acyl-CoA synthetase 5. *Histol Histopathol* 2005;20:409–14.
41. Campbell JD, Mazzilli SA, Reid ME, et al. The case for a pre-cancer genome atlas (PCGA). *Cancer Prev Res (Phila)* 2016;9:119–24.